POLITECNICO DI TORINO
Repository ISTITUZIONALE

Micro-scale modeling of Lithium-ion battery

Original
Micro-scale modeling of Lithium-ion battery / Clerici, D., Mocera, F.. - In: IOP CONFERENCE SERIES: MATERIALS SCIENCE AND ENGINEERING. - ISSN 1757-8981. - 1038:(2021), p. 012007. (AIAS 2020 International Conference on Stress Analysis) [10.1088/1757-899x/1038/1/012007].

Availability:
This version is available at: 11583/2972270 since: 2022-10-12T16:49:19Z

Publisher:
IOP PUBLISHING LTD

Published
DOI:10.1088/1757-899x/1038/1/012007

Terms of use:

This article is made available under terms and conditions as specified in the corresponding bibliographic description in the repository

Publisher copyright

(Article begins on next page)

11 October 2026

PAPER • **OPEN ACCESS**

Micro-scale modeling of Lithium-ion battery

To cite this article: D Clerici and F Mocera 2021 *IOP Conf. Ser.: Mater. Sci. Eng.* **1038** 012007

View the article online for updates and enhancements.

You may also like

- Microscopy and Spectroscopy of Lithium Nickel Oxide-Based Particles Used in High Power Lithium-Ion Cells
D. P. Abraham, R. D. Twesten, M. Balasubramanian et al.
- Diagnostic Analysis of Electrodes from High-Power Lithium-Ion Cells Cycled under Different Conditions
K. A. Striebel, J. Shim, E. J. Cairns et al.
- Electrochemical Cycle-Life Characterization of High Energy Lithium-Ion Cells with Thick $Li(Ni_{0.6}Mn_{0.2}Co_{0.2})O_2$ and Graphite Electrodes
Yongjun Leng, Shanhai Ge, Dan Marple et al.

This content was downloaded from IP address 130.192.232.210 on 21/02/2023 at 09:21

Micro-scale modeling of Lithium-ion battery

D Clerici and F Mocera

Department of Mechanical and Aerospace Engineering, Politecnico di Torino, Corso duca degli abruzzi 24

E-mail: davide.clerici@polito.it

Abstract. Good energy density, long lifetime, high capacity and high voltage make Lithium-ion batteries the most widespread energy storage systems, suitable for several fields of application. Nevertheless, usage leads to cell degradation which mainly results in capacity and power fade. Degradation phenomena are the result of the interaction between mechanical and electro-chemical mechanisms, which are reviewed in this paper. Lithium-ion batteries store and deliver electric energy by means of ions transport between anode and cathode through the electrolyte. The active material of the electrodes consists of micrometer particles which can host lithium ions through insertion/extraction processes. These processes are modelled as diffusion-mechanical problem, since the lithium concentration gradient within the particle due to ions diffusion generates internal stresses in analogy with a temperature gradient. The model in this work, usually referred as diffusion induced stress (DIS), can predict the stresses in the active material particles which are the driving force for damage, pulverization, exfoliation and crack propagation. Indeed, the damage induced by the insertion/extraction processes explains the capacity reduction over charge/discharge cycles: a critical issue for batteries lifetime.

1. Introduction

Lithium-ion batteries are the most widespread rechargeable energy-storage systems and they have a large field of application from small electronic systems up to electric vehicles in automotive and industrial applications [1]. Indeed, they can span a great capacity and power range with a good energy density and long lifetime. Actually, the main drawbacks are related to safety and performance through whole life cycle [2, 3]. Indeed, materials which guarantee good nominal performance, such as capacity, energy and power density, could be subjected to faster degradation and shorter lifetime. As a consequence, the study of cells damaging is a key issue for developing innovative materials, folding and housing technique which can improve the performance of current Li-ion cells. Damaging can be due to several phenomena, as illustrated in figure 1.

Most of the literature works focuses on the electrochemical phenomena, such as decomposition of active material and its performance in the voltage window of the cell. But an increasing attention has been paid in the last years to the mechanical phenomena involved in Lithium-ion cell, which can be mainly divided in two categories: Thermal phenomena and Diffusional phenomena. Thermal phenomena are due to the differential thermal strain which establishes in the cell during usage [4]. Diffusional phenomena are due to intercalation and deintercalation of Lithium ion in the active material via electro-chemical reactions. Their study has started with the works of Newman and Christensen [5, 6, 7] in recent years. Diffusional phenomena must be studied at micrometer scale, because active materials of anode and cathode are made

Content from this work may be used under the terms of the Creative Commons Attribution 3.0 licence. Any further distribution of this work must maintain attribution to the author(s) and the title of the work, journal citation and DOI.
Published under licence by IOP Publishing Ltd

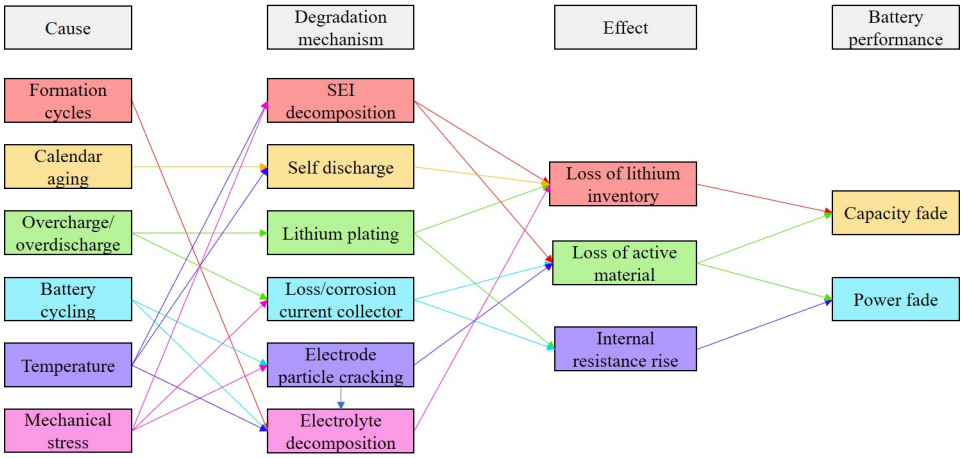

Figure 1. Main damaging mechanisms.

of micrometer particles which can host and release Lithium ions during cell operation, as shown in figure 2.

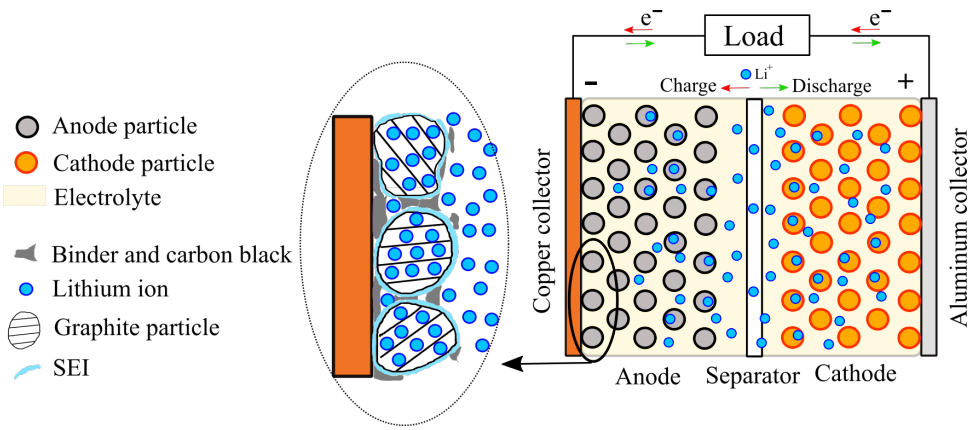

Figure 2. Main damaging mechanisms [8].

Lithium-ions give rise to mechanical stresses when they occupy or leave (according to insertion or extraction process) an interstice in the active material particles. The aforementioned mechanical stresses damage the active material structure, leading to crack growth, pulverization and material loss. The damage and the cracks in the active material leads to material isolation, loss/fragmentation and solid electrolyte interphase (SEI) growth, which results in capacity reduction over charge/discharge cycles. In particular, the combination of mechanical and electrochemical phenomena related to crack propagation and SEI growth, is the main source of damage. SEI is a thin film made of the products of the electrolyte decomposition which occurs on the interphase between electrolyte and active material particles. The decomposition reaction consumes lithium ions, which are no more available to be cycled, thus, the battery capacity decreases. The decomposition occurs mainly during the first cycles, and then slows down as the interfaces between active material and electrolyte are covered by the SEI layer. However, if the active material is being damaged during the cell operation, the SEI layer can grow on the new surfaces created by the crack and the capacity fade continues even after the first cycles, as qualitatively explained in figure 3.

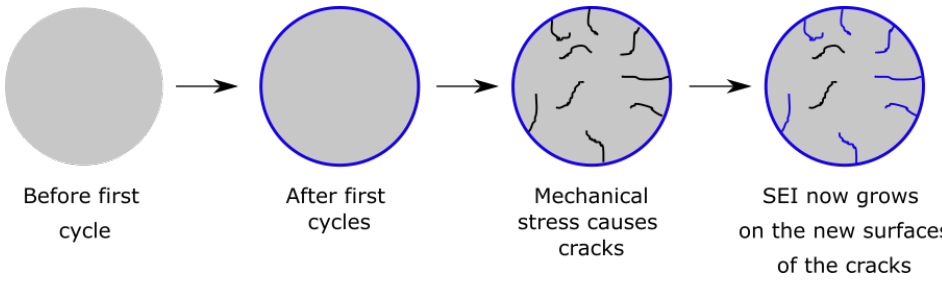

Figure 3. Cracks growth/SEI decomposition mechanism. The grey circle represents a particle in the active material, the blue lines represents the SEI layers, the black lines represents the cracks.

In this paper a review of the nature and the source of the stresses which arise in Lithium-ion battery is presented. This type of stresses are computed with an analytical procedure in section 2.1, which is then used to validate the FEM model formulated according to the thermal-diffusional analogy in section 2.3.

2. Method

2.1. Analytic method

Common active materials of anode and cathode in Lithium Ion Batteries can be assumed, under reasonable hypothesis [8], like a frame of spherical particles, as shown in figure 2. When approaching active material, Lithium ions give rise to electrochemical reactions: an electron flows in the host material and a Lithium ion is inserted in an interstitial sites of the active material particle in case of insertion. On the contrary, during extraction a Lithium ion is deintercalated from the interstitial site of the active material particle and an electron is released simultaneously. Now, focusing on the insertion process, Lithium ions approach the external surface of the particle and gradually diffuse towards the core, so that the interstitial sites close to the surface are available to accommodate new ions. This fact makes the lithium concentration inside the active material particles inhomogeneous along radial coordinate, a greater lithium concentration is expected on the surface, which gradually fades off towards the core during lithium insertion, as shown in figure 4a.

On the contrary, during extraction Lithium ions are removed from the surface of the particle and the ions are gradually retrieved from the core, this results in a greater lithium concentration in the core which fades off towards the surface, as explained in figure 4b. Concentration inhomogeneity, in analogy with temperature gradient, causes differential strains among areas characterized by different concentration levels, according to the law established by Prussin [9].

$$\varepsilon_{ch} = \Omega(C - C_{ref}) \tag{1}$$

Where ε_{ch} is the chemical deformation induced by the lithium ion concentration gradient. Ω is the partial molar volume of lithium in the host material and describes the volume increase of the host material per unit of solute (Lithium) mole. An increasing concentration causes a volume increment for material with positive partial molar volume. C_{ref} is the concentration value which corresponds to zero strain in the active material.

The concentration inhomogeneity, highlighted in figure 4, produces a mismatch in the deformation along the radius of the particle, which leads to internal stress. In insertion, referring to Figure 4a, the greater concentration of the outer layers causes a tensile radial stress all over the particle because the surface expands more than the core. The hoop stress is compressive in the outer layers and tensile in the core because the greater deformation of the surface is

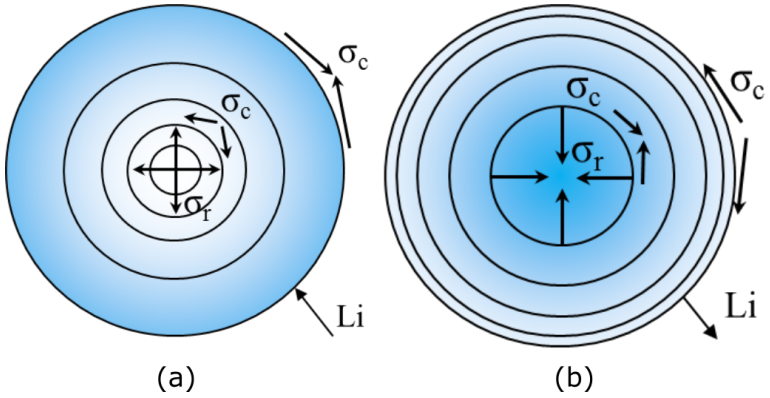

Figure 4. Stress and deformation of the active material particles during lithium insertion (a) and extraction (b). Blue shadows depict the lithium concentration (blue means high concentration, white means low concentration). Concentration level affects tension (arrows pointing toward each other) and compression (arrows pointing away from each other) of radial and hoop stress. The concentric lines show expansion or shrinking of the particle: they are evenly spaced in the undeformed configuration.

prevented by the core. In extraction (Figure 2b) the particle shrinks, and the radial stress is compressive because the concentration level decreases along the radius. The hoop stress is tensile in the surface and compressive in the core because the greater expansion of the core is prevented by outer layers which are characterized by a lower concentration level. The signs of the stresses are reverted for materials with negative partial molar volume.

The details of the model derivation are presented in a previous paper and are not repeated here [8]. This type of problem, usually referred as diffusion induced stress (DIS), can be split in a mechanical and a diffusional aspect. The assumption of spherical geometry and isotropic and linear elastic material, deepened in [8], allows to derive a one-dimensional model in the radial coordinate, and to decompose the stress in radial and tangential component. The elastic problem is formulated defining the constitutive equations $(2a)$-$(2b)$, which consider both the elastic and chemical strain, the congruency equations $(2c)$ and the stress equilibrium over a spherical domain $(2d)$ [8].

$$\sigma_r = \frac{E\left[\left(\varepsilon_r - \frac{\Omega C}{3}\right)(1-\nu) + 2\nu\left(\varepsilon_c - \frac{\Omega C}{3}\right)\right]}{(1+\nu)(1-2\nu)} \tag{2a}$$

$$\sigma_c = \frac{E\left[\left(\varepsilon_c - \frac{\Omega C}{3}\right) + \nu\left(\varepsilon_r - \frac{\Omega C}{3}\right)\right]}{(1+\nu)(1-2\nu)} \tag{2b}$$

$$\varepsilon_r = \frac{du}{dr}, \quad \varepsilon_c = \frac{u}{r} \tag{2c}$$

$$\frac{d\sigma_r}{dr} + \frac{2}{r}\left(\sigma_r - \sigma_c\right) = 0 \tag{2d}$$

Where E and ν are Young modulus and Poisson ratio of the host material and r is the radial coordinate. The combination of $(2a)$-$(2d)$ leads to a second order differential equation in the displacement with constant coefficients (3).

$$\frac{d^2u}{dr^2} + \frac{2}{r}\frac{du}{dr} - \frac{2u}{r^2} = \frac{1+\nu}{1-\nu}\frac{\Omega}{3}\frac{dC}{dr} \tag{3}$$

The right hand side of the equation represents the forcer of the equation and depends on the Lithium concentration at radius r and on the mechanical properties of the material. The solution of the mechanical problem (4) is got integrating twice (3) and imposing null displacement at the centre of the sphere and free expansion at the surface ($\sigma_r(R) = 0$).

$$u(r) = \frac{\Omega}{3(1-\nu)}\left[(1+\nu)\frac{1}{r^2}\int_0^r C(r)r^2\,dr + 2(1-2\nu)\frac{r}{R^3}\int_0^R C(r)r^2\,dr\right] \tag{4}$$

(4) predicts the displacement of the points inside the particle at radius r, given the concentration distribution all over the particle. (4) depends only on the Lithium concentration and on the mechanical properties of the host material. At this stage, the concentration distribution must be computed to get the solution of the DIS problem. The concentration field within the particle is computed according to the diffusion equation (5).

$$\frac{\partial C}{\partial t} = \nabla \cdot (D\nabla C) \tag{5}$$

Where D is the diffusion coefficient of Lithium in the host material and describes how fast the ions move in the host structure. Lithium concentration is itself the driving force of lithium ions flow across the domain in (5). Indeed, under the effects of the boundary conditions, lithium ions flows from areas with high concentration to areas with lower concentration. (5) is associated with a couple of possible boundary conditions, according to two possible cell operation, resumed in ($6a$)-($6b$): galvanostatic (constant current) or potentiostatic (constant voltage) operation. A constant Lithium ion flux equal to the current density divided by the Faraday constant (F) is applied on the external surface of the particle when the cell is charged or discharged with a constant current ($6b$), then the flux is set to zero at the centre of the particle according to the axisymmetric nature of the problem. A constant concentration equal to the solubility limit is imposed on the external surface of the particle when the cell is charged or discharged with constant voltage ($6a$), and a finite concentration value is prescribed at the centre of the particle.

$$\begin{cases} C(r,0) = C_0, & \text{for } 0 \le r \le R \\ C(R,0) = C_R, & \text{for } t \ge 0 \\ C(0,t) = finite, & \text{for } t \ge 0 \end{cases} \tag{6a}$$

$$\begin{cases} C(r,0) = C_0, & \text{for } 0 \le r \le R \\ \left.\dfrac{\partial C(r,t)}{\partial r}\right|_{r=R} = \dfrac{I}{FD}, & \text{for } t \ge 0 \\ \left.\dfrac{\partial C(r,t)}{\partial r}\right|_{r=0} = 0, & \text{for } t \ge 0 \end{cases} \tag{6b}$$

At this stage the concentration distribution as a function of time can be derived via variable separation, and the final result is shown in ($7a$)-($7b$) for potentiostatic and galvanostatic operation, respectively [10].

$$\frac{C(r,t) - C_R}{C_0 - C_R} = -2\sum_{n=1}^{\infty}\frac{(-1)^{n+1}}{\pi n x}\,sin(n\pi x)\,e^{-n^2\pi^2\tau} \tag{7a}$$

$$C(r,t) = C_0 + \frac{IR}{FD}\left[3\tau + \frac{x^2}{2} - \frac{3}{10} - \frac{2}{x}\sum_{n=1}^{\infty}\left(\frac{sin(\lambda_n x)}{\lambda_n^2 sin(\lambda_n)}e^{-\lambda_n^2\tau}\right)\right] \tag{7b}$$

A more accurate model, referred as "coupled problem", considers the dependence of the chemical diffusion on the stress. Indeed, lithium ions are rejected from areas with compressive stress and attracted in areas with tensile stress. Therefore, this model considers two driving forces for lithium diffusion: concentration and stress. The stress driving force is expressed through an equivalent diffusion coefficient, which is given in (8) after some arrangements, and replaces the physical diffusion coefficient D.

$$D_{eqv} = D\left(1 + \frac{2\Omega^2 E}{9R_g T(1-v)}C\right) = D(1 + Y \cdot C) \tag{8}$$

The equivalent diffusion depends in turn on the concentration, so the solutions $(7a)$-$(7b)$ becomes non-linear and the diffusional and mechanical fields tightly coupled.

The reader is suggested to check a previous paper [8] for clear details about this argument.

At this stage, once the concentration field is computed along with its time evolution according to the uncoupled or the coupled model, the displacement, strains and stresses field can be computed with equations (3)-$(2c)$-$(2a)$-$(2b)$ for every time steps.

2.2. Thermal analogy

The multi-physics problem explained in section 2.1 can be studied as a mechanical/thermal system instead of a mechanical/diffusive system, exploiting the analogy between the diffusive and thermal equations. The advantage of this choice is the readiness of implementing a mechanical/thermal problem in a commercial finite element software.

Ideally, equating the diffusional strain due to inhomogeneity in chemical concentration with the thermal strain (9), an equivalent temperature gradient, which induce the same strain induced by the concentration one, is got.

$$\alpha(T - T_{ref}) = \frac{\Omega}{3}(C - C_{ref}) \Rightarrow T = T_{ref} + \frac{\Omega}{3\alpha}(C - C_{ref}) \tag{9}$$

Where α is the thermal expansion coefficient, $\frac{\Omega}{3}$ is the volume expansion due to concentration inhomogeneity, T_{ref} and C_{ref} are temperature and concentration referred to zero strain. The temperature field computed with (9) can be assigned to the body, in order to produce the correct strain due to the external chemical load.

At this stage the concentration field, replaced by the equivalent thermal one, is left to be computed. This step is accomplished analysing the analogy between the equations which describes the two phenomena, reported in table 1.

Table 1. Analogy between thermal and diffusive equations.

Type	Heat	Diffusion
Conservation equation	$\frac{\partial T}{\partial t} = \nabla \cdot (\gamma \nabla T)$	$\frac{\partial C}{\partial t} = \nabla \cdot (D \nabla C)$
Flux	$J_T = -k\nabla(T)$	$J_C = -D\nabla(C)$
Equivalent diffusion	$k_{eqv} = k(1 + Y \cdot T)$	$D_{eqv} = D(1 + Y \cdot C)$

Conservation equations (first line of table 1) are equivalent if thermal diffusion (γ) is equal to chemical diffusion (D). Then, considering the flux (second line of table 1), thermal conductivity k must be equal to chemical diffusion. Since both thermal diffusion and thermal conductivity

must be equal to chemical diffusion, and thermal diffusion is expressed as $\gamma = \frac{k}{\rho c_p}$ the condition for thermal/chemical analogy is:

$$\gamma = \frac{k}{\rho c_p} \quad \Rightarrow \quad k = D \wedge \rho c_p = 1 \tag{10}$$

If (10) holds, the concentration field can be replaced by the temperature one, and the two phenomena are written in analogy.

The "coupled problem" is implemented with the thermal analogy defining a thermal conductivity coefficient depending on temperature. In this way also the thermal diffusion depends on temperature, as the equivalent chemical diffusion depends on concentration, according the third line of table 1.

2.3. FEM

The thermal/chemical analogy allows to deal the multi-physics problem explained in section 2.1 in a numerical way [11] with the commercial finite element software Ansys. Indeed, the multi-physics capability of Ansys can be exploited to get the solution in a convenient way. The direct application of (9) assumes that the chemical distribution is already known, so it must be computed in an analytical or numerical way before starting the mechanical computation. Instead, Ansys can solve the thermal and mechanical problem in a single analysis, even simultaneously. The thermal problem is solved according to the boundary conditions (6*a*)-(6*b*) of the systems described in section 2.1. The galvanostatic operation consists of a constant lithium flux at the edge of the particle, which is simulated with a constant heat flux computed according to the thermal analogy, referring to second line of table 1. The potentiostatic operation consists in assigning the maximum concentration value (referred to the saturation limit) at the edge of the particle, this is simulated with a Dirichlet condition, i.e. a constant temperature, computed according to the thermal analogy (9).

The "coupled" problem is treated assigning to the body a parametrized value of thermal conductivity, as summarized in the third line of table 1. The thermal conductivity varies linearly with the temperature with the coefficient Y, which contains just constant parameter of the problem. It is highlighted that the temperature in the coefficient Y is the real ambient temperature, and is treated as a constant for our purpose.

Therefore, displacements, strains and stress are computed as a consequence of the external load, i.e. the chemical concentration distribution modelled as a temperature one.

3. Results

3.1. Numerical model validation

In this section the results obtained with the numerical model are validated by the results derived with the analytical model. The physical parameter of lithium manganese oxide (LMO), a common cathode material, are fed into the model and are summarized in table 2.

Table 2. Material properties LMO.

Parameter	Symbol	Value	Unit
Young Modulus	E	15	GPa
Poisson ration	ν	0.3	-
Maximum concentration	C_{max}	$2.29\,10^{4}$	mol/m^3
Fraction molar volume	Ω	$3.497\,10^{-6}$	m^3/mol
Particle radius	R	$5\,10^{-6}$	m

A thermal-mechanical analysis was implemented in ansys workbench exploiting the thermal analogy, a sketch of the system is given in figure 5.

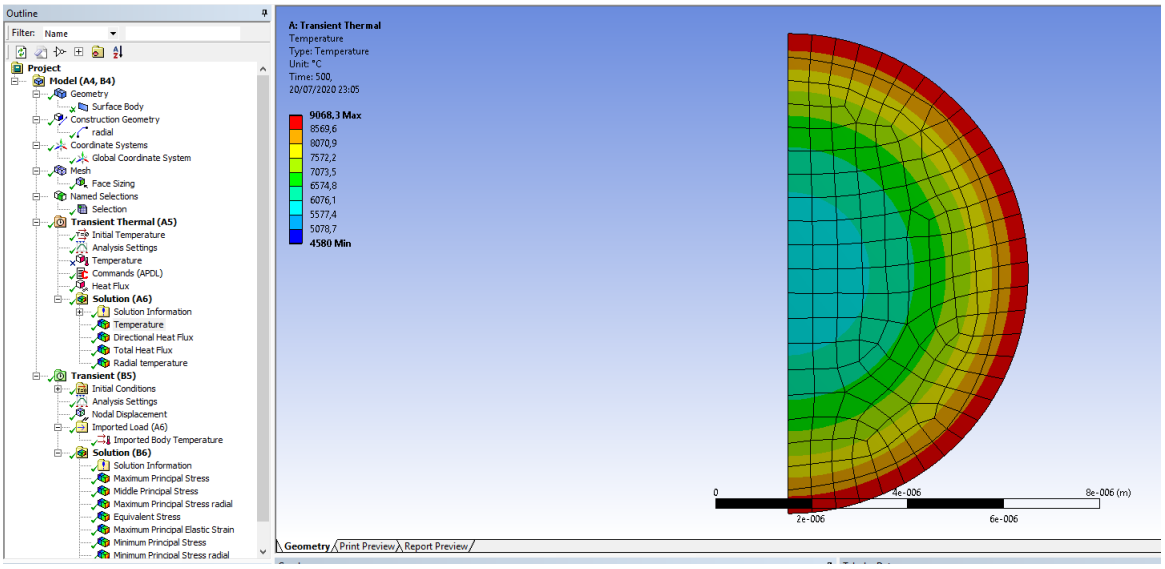

Figure 5. Axysimmetric model in Ansys and equivalent temperature distribution.

The results are validated with the analytical model implemented in MATLAB feeding the same input parameter, and the comparisons between concentration and stresses are given in figure 6.

A good agreement between numerical and analytical model in galvanostatic operation is shown by the comparison presented in figure 6.

Therefore the numeric model is validated with the analytical model in figure 7 in potentiostatic operation, which shows a good agreement between the two model even in this type of operation.

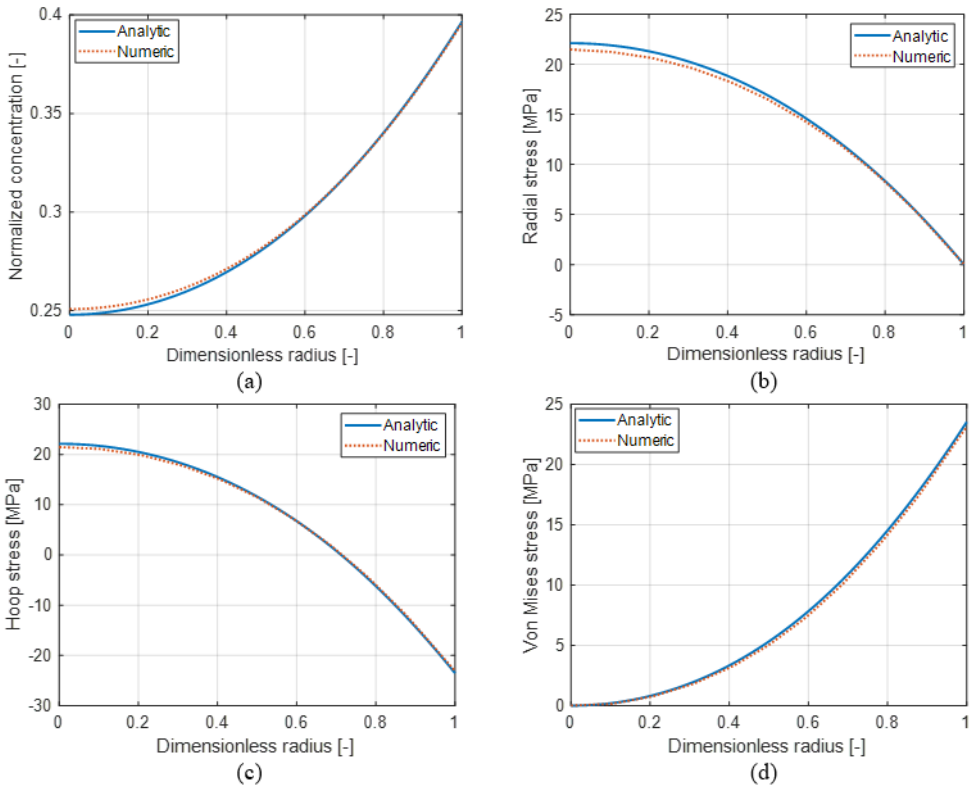

Figure 6. Comparison between analytical and numerical (FEM) results of concentration and stresses in galvanostatic operation. The simulation time is equal to 500s. Normalized concentration is given as C/C_{max}, dimensionless radius is given as r/R.

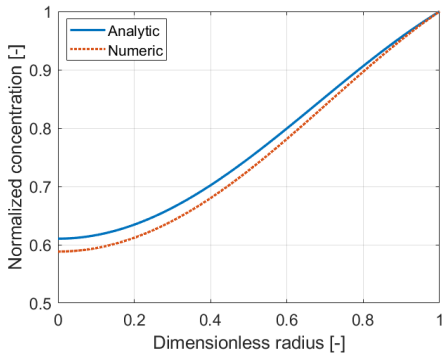

Figure 7. Comparison between analytical and numerical (FEM) results of concentration in potentiostatic operation. The simulation time is equal to 500s. Normalized concentration is given as C/C_{max}, dimensionless radius is given as r/R.

3.2. Evolution in time

At this stage the concentration and stress are computed with different state of charge (SOC), in order to explore how they vary during cell charging. This has been done varying the simulation time in case of Lithium-ion insertion. The results of galvanostatic operation are showed in figure 8.

The concentration variation in figure 8a shows how the lithium concentration level grows up in

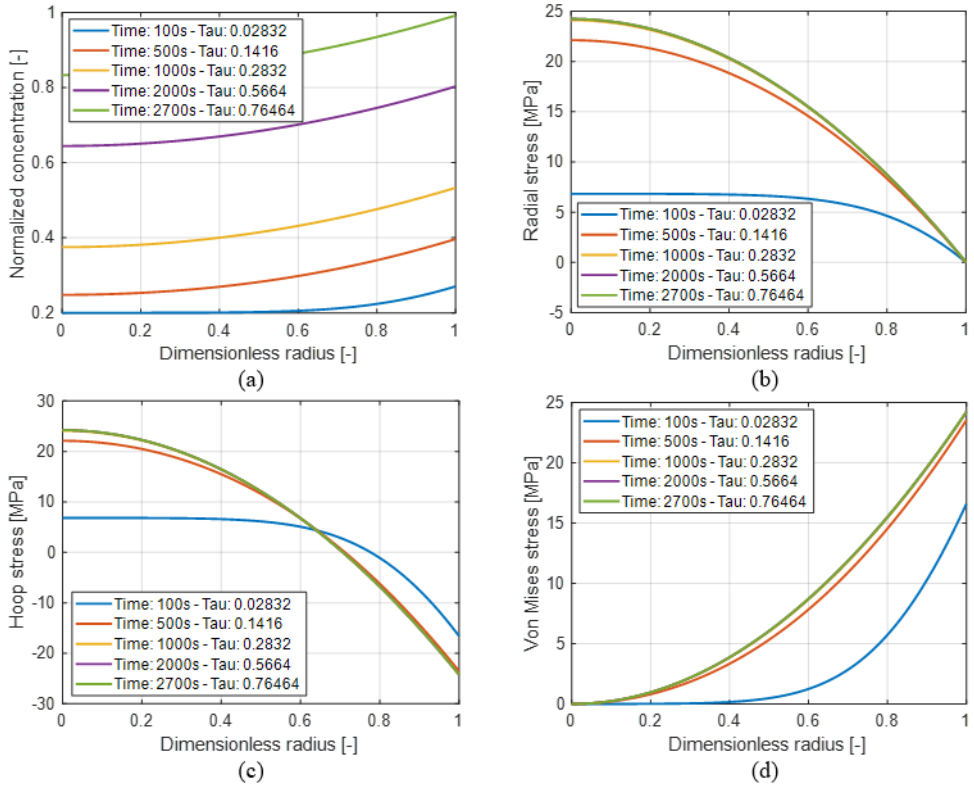

Figure 8. Evolution of concentration and stress in time in galvanostatic operation. Normalized concentration is given as C/C_{max}, dimensionless radius is given as r/R.

the active material particle with increasing simulation times. The surface concentration reaches the solubility limit (C_{max} or normalized concentration $C/C_{max} = 1$) after 2700s for a LMO particle with the physical properties reported in table 2, after this time the simulation must be conducted according to potentiostatic operation, namely controlling the surface concentration value.

Radial stress, hoop stress and Von Mises stress are reported in figure 8b-d. Short after the beginning of the process the stresses trend keeps to the same level through the whole operation. Radial stress and hoop stress are equal at the centre of the particle, which is subjected to hydrostatic stress subsequently. As a result, the Von Mises stress is null at the centre of the particle and reaches it maximum value at the particle surface, where damage and crack propagation are likely to occur. In case of extraction, radial stress and hoop stress reverts their signs, therefore radial stress is compressive and hoop stress is compressive in the core and tensile on the surface of the particle, which can concur in crack growth according to mode I.

In the end, a characteristic charging method constant current/constant voltage is simulated, switching from galvanostatic to potentiostatic operation when the surface concentration reaches the solubility limit (after 2700s). The concentration and stresses results are reported in figure 9.

The current density adopted in simulation ($1A/m^2$) is really close to 1C, since after 3600s the concentration level is almost equal to the saturation level. An increase in radial and hoop stress is detected close to end of the charge during the potentiostatic operation, which reflects also in the Von Mises stress. Instead, Von Mises stress shows a peak about $0.9R$, and a lower value on the surface during potentiostatic charging. At the end of the charge the concentration distribution is flat, thus the decreasing of the concentration gradient reflects in lower stress

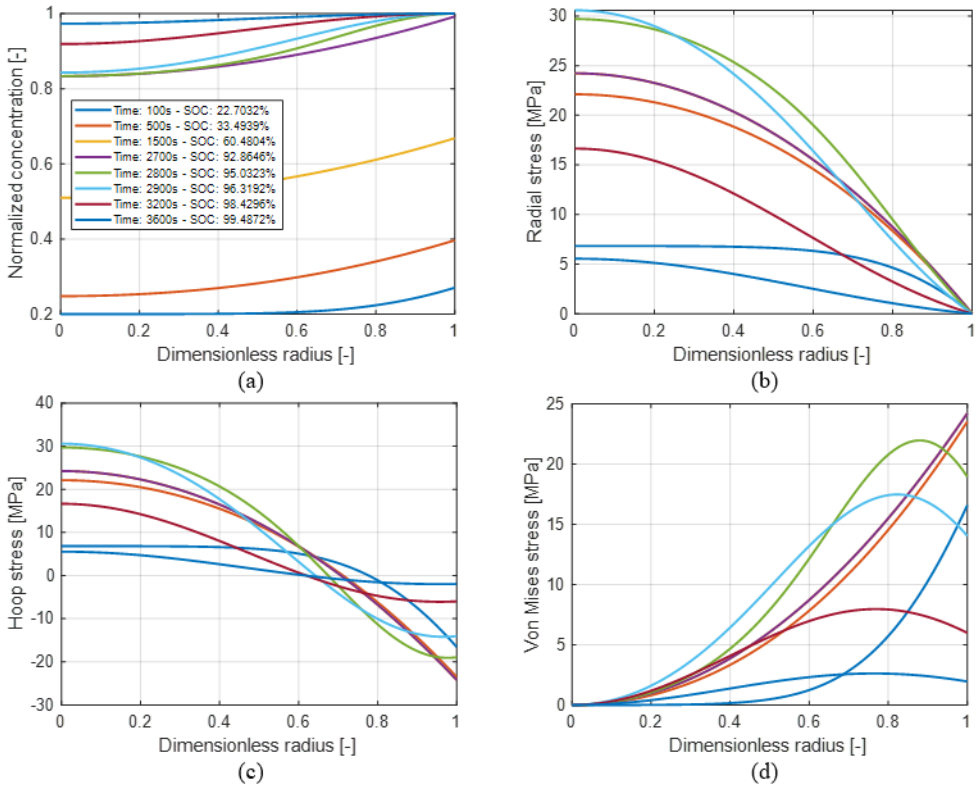

Figure 9. Charging simulation according to constant current - constant voltage method. The switch between the two operation occurs after 2700s, when surface concentration reaches the solubility limit (C_{max}). Normalized concentration is given as C/C_{max}, dimensionless radius is given as r/R.

values for SOC over 98%.

Different simulations were carried out with different charging rate, which is controlled varying the current density over the particle surface. The results shows, as expected, that higher lithium flux at the particle boundaries causes a higher concentration gradient which increases the stress inside the particle. In particular a maximum Von Mises stress value of 47 MPa, 70 MPa and 110MPa was observed for simulation carried out with a current density of 2 A/m^2, 3A/m^2 and 5A/m^2, respectively.

4. Conclusion

In this paper the authors had highlighted the importance of mechanical phenomena inside a Lithium-ion cell and how these phenomena are related to battery damaging. Indeed, Lithium ions intercalation/deintercalation inside the active material causes internal stress because of their inhomogeneous distribution during the diffusion process. An inhomogeneous mass distribution causes a chemical strain in analogy to an inhomogeneous temperature distribution, and a stress state within the active material consequently. The stress within the active material is the cause for pulverization, crack growth and damaging of the material, which reflects in a decrease of the cell performance. For this reason, quantifying the stress for a given active material with defined operation condition is a crucial issue to estimate the damaging and the cell lifecycle. Furthermore, an analytical model for stress computation is presented. The model follows a multi-physics approach, since the chemical distribution caused by lithium diffusion has to be

computed in order to get the stress. Moreover, concentration and stress are tightly coupled in the "coupled" model, since the concentration itself depends on the stress, and the solution procedure becomes non-linear.

The analogy between thermal strain and chemical strain is exploited to implement a numerical model of the problem in the commercial finite element software Ansys. Indeed, the numerical value of the thermal solution is equal to the concentration value and cause the same strain and stress if the physical and fictitious parameters are tuned properly. In this way the numerical solution can be got exploiting the multi-physics capability of Ansys. The results of the numerical model are validated with the established analytical model, and the fitting is satisfactory. Numerical modelling is the only way to perform simulation with different domain geometry or more complex boundary condition, which makes the assumptions necessary to derive the analytical model fall.

The results show that after few minutes from the beginning of the charge the stress distribution remains constant in the particle, and then a slight increase is detected during the potentiostatic operation at the end of the charge. The Equivalent stress value increases with the charging rate and can approach the yield stress of the material, this means that faster charge (or discharge) leads to a faster cell degradation.

Table 3. List of Symbols

Symbol	Parameter	Unit
C	Concentration	mol/m^3
C_0	Initial concentration	mol/m^3
C_{max}	Maximum concentration	mol/m^3
C_R	Surface concentration	mol/m^3
C_{ref}	Zero strain concentration	mol/m^3
D	Diffusion coefficient	m^2/s
D_{eqv}	Equivalent diffusion coefficient	m^2/s
E	Young Modulus	MPa
F	Faraday constant	96485.332 As/mol
I	Current density	A/m^2
r	Radius	m
R	Particle radius	m
R_g	Gas constant	8.3145 $J/molK$
SOC	State of charge	-
T	Temperature	$298K$
T_{ref}	Zero strain temperature	$273K$
u	Displacement	m
x	Normalized radial coordinate	-
ϵ_c	Hoop strain	-
ϵ_{ch}	Chemical strain	-
ϵ_r	Radial strain	-
λ_n	Roots of trascendent equation $\lambda = tan(\lambda)$	-
υ	Poisson ratio	-
σ_c	Hoop stress	MPa
σ_r	Radial stress	MPa
τ	Characteristic time	D/tR^2
Ω	Partial molar volume	m^3/mol

References

[1] Somà A 2016 Hybridization factor and performance of hybrid electric telehandler vehicle. *IEEE Trans. Ind. Appl* **52** 5130-38
[2] Mocera F 2019 Battery performance analysis for working vehicles applications. *IEEE Trans. Ind. Appl* **56**644-653
[3] E. Vergori, 2018 Battery modelling and simulation using a programmable testing equipment. *Computers* **7**
[4] Mocera F, Vergori E and Somà A, 2018 Finite element versus experimental Thermo-mechanical behaviour of prismatic Li-Ion cell. *IEEE Conf. EVER 2019* 1-8
[5] Christensen J and Newman J 2006 Stress generation and fracture in lithium insertion materials. *J. Solid State Electrochem.* **24** 222

[6] Christensen J and Newman J 2006 A mathematical model of stress generation and fracture in lithium manganese oxide. *J. Electrochem. Soc.* **153** 1019-1030
[7] Christensen J 2010 Modeling diffusion-induced stress in Li-ion cells with porous electrodes. *J. Electrochem. Soc.* **157** 336-386
[8] Clerici D, Mocera F and Somà A, 2020 Analytical Solution for Coupled Diffusion Induced Stress Model for Lithium-Ion Battery. *Energies* **13** 1717
[9] Prussin S 1961 Generation and distribution of dislocations by solute diffusion. *J. Appl. Phys.* **32** 1876-81
[10] Cheng Y and Verbrugge M 2009 Evolution of Stress within a Spherical Insertion Electrode Particle Under Potentiostatic and Galvanostatic Operation. *J. Power Sources* **190** 453-460
[11] Zhang X, Shyy W and Sastrya M 2007 Numerical Simulation of Intercalation-Induced Stress in Li-Ion Battery Electrode Particles. *J. Eelectrochem Soc* **154** 910-916